UNIVERSITY of CALIFORNIA

SANTA CRUZ

Rapidity Distribution Comparisons Between $t\bar{t}$ and W+4jets Signals At The LHC Using Simulated Data

A Thesis Submitted in Partial Satisfaction
Of the Requirements for the Degree of

BACHELOR OF SCIENCE

in

PHYSICS

by

Jesse G. Sherer

June 10, 2009

The thesis of Jesse G. Sherer is approved by:

_____	_____
Jason Nielsen Technical Advisor	David P. Belanger Advisor of Senior Theses

_____
David P. Belanger
Chair, Department of Physics

Abstract

Rapidity Distribution Comparisons Between $t\bar{t}$ and W+4jets Signals At The LHC Using Simulated Data

by

Jesse G. Sherer

In this we shall introduce and describe the necessary concepts required in order to investigate the rapidity asymmetry distribution of W+4jets as compared to that of $t\bar{t}$ in theory and experiment. Beginning with the leptonic W+0jets, we run simulated events using MadGraph/MadEvent at the theory level, and build up through PYTHIA and PGS to the experimental level. We then progressively add on additional jets and repeat the generation procedure from the beginning until we have built up to W+4jets. At this point we are able to make comparisons with the semi-leptonic $t\bar{t}$ rapidity distribution in order to attempt to make fits of the respective signals.

Contents

Dedication **5**

Acknowledgements **6**

1. Motivation **8**
2. Particle Physics **9**
2.1 Standard Model Overview 9
2.2 Weak Interactions 12
2.2.1 Neutral Current Reactions 13
2.2.2 Charged Current Reactions 13
2.2.2.1 The CKM Matrix 15
2.3 Strong Interactions and Hadronic Physics 16
2.3.1 The Parton Model 16
2.3.2 Quark Model 16
2.3.2.1 Valence and Sea Quarks 17
2.3.2.2 Parton Distribution Functions 17
2.3.2.3 QCD Background 20
2.3.3 Hadronic Jets 20
3. Methods **21**
3.1 The ATLAS Detector 22
3.1.1 Triggering 23
3.1.2 Event Reconstruction 24
3.2 Simulation Methods 26
3.2.1 MadGraph/MadEvent 27
3.2.2 PYTHIA 28
3.2.3 PGS 29
4. Phenomenology **30**
4.1 $W^{\pm}$ Production 30
4.2 Top Production 32
5. Results and Analysis **34**
5.1 Theory Results 35
5.2 Experimental Results 38
5.3 Fitting 40
6. **Conclusion** **41**

Appendix **42**

References **43**

Dedication

I dedicate this thesis to Odin.

Acknowledgements

With this thesis effectively as my last academic act as an undergraduate, I would like to thank all of those who have helped me get to where I am today. My parents, for their constant love and support throughout all my endeavors. To Evelynn, for her support and companionship during a tremendous transition in my life. My classmates, without whom my education would have been far more challenging, and far less fulfilling. For Trader Joe's Palm Desert, whose mortifying prospect spurred me to get my life in order and go back to school. The fnord.

I would like to sincerely thank Professor Jason Nielsen for his time and energy in helping acquaint me with the realm of experimental high energy physics, without whom this thesis would not exist.

1. Motivation

The goal of this research was to investigate the phenomenology of W boson production with the ATLAS detector at the Large Hadron Collider (LHC) as a background for $t\bar{t}$, and in turn for $t\bar{t}$ production as a background for W. We did this through using Monte Carlo simulation software designed to emulate the ATLAS detector environment. Specifically, we were interested in the rapidity asymmetry between the direct production of W^+ and W^-, starting at the theory level and ending at the "pretty good simulation" (PGS) level, and whether or not the distribution could be fitted as a background from a signal. We did this starting at the matrix element calculations using MadGraph and proceeding to simulate the outgoing particles with MadEvent. From there we used the hadronic showering program Pythia, and then the ATLAS detector emulator PGS.

The rapidity asymmetry can be seen in W^- production as a very broad symmetric signal peaked at $\eta = 0$, while in W^+ production it manifests itself as a pair of "horns" that, although are symmetric about $\eta = 0$, peak away from 0 in negative and positive η. In investigating the rapidity distribution of the leptons produced by the W decays, we looked at the processes W+njets, where n = 0, 1, 3, 4. The interest was in whether or not the lepton rapidity reflected the parent W rapidity, and whether the W rapidity itself changed from the basic process of W+0jets. W+4jets is of particular interest in that it creates a background for the semi-leptonic top quark decay mode, which is itself a background in the lepton+jets+missing transverse energy channel. This is an important physics channel at the LHC for physics searches beyond the standard model.

To make our comparisons we also generated a sample of semi-leptonic top decays. Our ultimate goal was to test whether or not, using our observed rapidity distributions, we could subtract out the signals from a combined background of different process signals.

We produced all of our data using Monte Carlo simulation software at the matrix element level with MadGraph, parton level with MadEvent, parton showering and hadronization level with PYTHIA, and at the simulation level with PGS.

2. Particle Physics

As this research is in the field of high energy particle physics, a brief overview of the Standard Model is in order.

2.1 Standard Model Overview

The Standard Model of particle physics is the modern theory which outlines the behavior of the known fundamental particles – matter and force carriers. The simplest defining properties of particles are their spin, mass, electric charge, color charge, and the various conserved flavor quantum numbers of which lepton number and baryon number will be the most important for this discussion. Matter is separated from the force carriers based on the intrinsic spin of the particles – matter consisting of spin-½ fermions, as distinguished from the force carriers which are spin-1 gauge bosons. Matter is then divided into the leptons and hadronic quarks (baryons), each carrying their respective conserved quantum number and lacking the other.

The leptons are further divided into the charged leptons – the electron, muon, and tau, each with -1 times the elementary electric charge Q – and their respective neutrinos, the neutral leptons each with zero electric charge. The leptons each possess a lepton number of +1. The quarks are all electrically charged, with the up, charm, and top having +2/3 Q, and the down, strange, and bottom all having -1/3 Q. In a likewise association, the up, charm, and top quarks are regarded as "up-type quarks," while the down, strange, and bottom are regarded as "down-type quarks." The quarks, in addition, all carry a color charge – red, green, or blue. For quarks, their baryon numbers are each +1/3, so that a composite particle such as the proton (made up of two ups and a down quark) has a baryon number of +1.

For every fermion there is then an anti-matter partner which possesses opposite electric and color charge, lepton and baryon number, though with the same spin and mass as its matter counterpart. In the case of color charge, anti-quarks carry cyan, magenta, or yellow (anti-red, anti-green, or anti-blue respectively).

Another key element of the standard model is what is known as the particle generations. Both the leptons and quarks fall into one of the three generations of particles. The first generation consists of the electron and electron neutrino from the leptons, and the up and down quarks from the hadrons. The second generation consisting of the muon, muon neutrino, charm and strange quark, with the third consisting of the tau, tau neutrino, top and bottom quark.

One of the key features of the different particle generations is the conservation of the particle generation type. Namely, conservation of an electron, muon, or tau lepton number to replace the more general lepton number, and applies both to the charged and

neutral leptons. Similarly, there are conserved quantum numbers for each quark flavor, the most widely known being Strangeness, but also including Charmness, Bottomness and Topness. Another aspect of the particle generations is an increasing mass of the particles in subsequent generations. For instance, the mass of the electron is less than the mass of the muon which is less than that of the tau. This is especially true in the increasing mass of the subsequent quarks after up and down. Currently it is not known whether or not the neutrinos exhibit such a mass trend, as it has only recently been confirmed that any of the neutrinos exhibit a mass at all.

The other set of the known fundamental particles are the spin-1 gauge bosons, which are the fundamental force carriers. These consist of the electromagnetic carrier the photon, the strong carrier the gluon, and the weak carriers the $W^{\pm}$ and Z^0. The photon and gluon are both massless, neutral particles, of which the gluon additionally possesses color charge. The $W^{\pm}$ and Z^0 are both massive particles of which the W's are electrically charged, while the Z^0 is neutral. The weak and strong interactions will be discussed in more detail in subsequent sections. The possession or lack of color charge dictates whether or not a particle interacts through the strong force, just as the possession of an electric charge dictates whether or not a particle interacts through the electromagnetic force. In this way, it is said that a particle couples to one of the forces. For electromagnetism, the electric charge is a manifestation of this coupling to the electric field, while for the strong force possession of color charge represents a coupling to the strong field.

2.2 Weak interactions

The weak interaction is mediated by the spin-1 gauge bosons $W^{\pm}$ and the Z^0, which mediate the *charged* and *neutral* current reactions respectively. Unlike the strong and electromagnetic forces, the weak force carriers are massive particles with masses measured to be

$$M_W = 80.398 \pm 0.025 \text{ GeV and } M_Z = 91.1876 \pm 0.0021 \text{ GeV [1].}$$

Given these large masses, the Yukawa theory for massive force carriers [10, p.176] dictates that the weak force has a finite, and short, range given by the relation

$$R \equiv \hbar/Mc \quad (2.1)$$

where M is the mass of the force carrier. From this relation you can see that as the mass of the gauge boson goes to zero, the range of the force goes to infinity as is seen in electromagnetism (and in the strong force, which is however quite a bit more complicated). From this, given the mass of the $W^{\pm}$ for instance, the range of the weak interaction can be calculated to be approximately

$$R_W \equiv \hbar/M_W c \approx 2 \times 10^{-3}\text{fm [2, p.17]} \quad (2.2)$$

or, on the order of the size of an atomic nucleus. It is this interaction range which makes the weak force so "weak." The intrinsic strength of the weak interaction is on the order of that of electromagnetism, which makes sense in the modern concept of the unified electroweak theory. Martin and Shaw [2, p.204] give an order of magnitude estimate for $\alpha_W \approx 1/400$, which given $\alpha \cong 1/137$ is indeed of the same order.

The weak carriers hold a special historical significance in that the theory to describe them was developed before their discovery. In 1968 Glashow, Weinberg, and Salam put forward their electroweak theory which unified electricity and magnetism. In

this theory they predicted the existence of the $W^{\pm}$ as the particles behind the already known phenomena of weak decay, as well as a never before suggested particle the Z^0. In back to back discoveries in 1983, the UA1 and UA2 experiments at the Super Proton Synchrotron discovered the $W^{\pm}$ and Z^0 as predicted.

2.2.1 Neutral Current Reactions

The so-called neutral current reactions are mitigated by the Z^0. As Z^0's are neutral particles they must produce decay products with zero net charge, which would be any fermion with its antimatter partner. Unlike for photons, this includes neutrino-antineutrino pairs, as neutrinos do not couple to electromagnetism. Neutral currents are found more generally to conserve both specific generation lepton number (where the leptons have both equal, and opposite, or zero charge), but also specific generation quark number (i.e. Strangeness, etc.). Despite conserving charge, Z^0's will not decay to different generations of either up-type, or down-type quarks, as this could violate the specific generation quark numbers. Although Z^0's mediate many similar interactions as photons, and therefore can be found in replace of photons, they only do so at energies sufficiently high enough to produce particles with the Z^0's high mass.

2.2.2 Charged Current Reactions

The charged current reactions are regarded as the alchemist of the forces, responsible for converting between flavors of quarks, and between leptons and lepton neutrinos. In the conversion between quarks, either an up-type quark is converted into a down-type quark, or vice versa, depending on the charge of the W boson emitted or

absorbed. This conversion occurs most often between quarks of the same generation than between quarks of differing generations and is reflected in the Cabibbo–Kobayashi–Maskawa (CKM) Matrix to be discussed. In the leptonic conversions, a charged lepton is converted into a neutrino of the same generation, or vice versa, depending on the charge of the W boson emitted or absorbed. These basic processes can then also be applied to $W^{\pm}$ decay, where an emitted W decays into a fermion, antifermion pair. In this case it is either an up-type quark and an antidown-type quark, or a lepton and antineutrino (or with the matter and antimatter interchanged).

In particle interactions and decays, the charged current reactions can take one of three forms - purely leptonic, semi-leptonic, or purely hadronic, depending on what end state particles are present. As the names imply, the end state particles for a purely leptonic process are all leptons, the end states for semi-leptonic are leptons, quarks and antiquarks (hadrons), and for purely hadronic are only quarks and antiquarks. An example of a purely leptonic process is muon decay

$$\mu^- \rightarrow e^- + \bar{\nu}_e + \nu_\mu.$$

An example of a semi-leptonic process is nuclear beta minus decay

$$\mathrm{n} \rightarrow \mathrm{p} + e^- + \bar{\nu}_e.$$

A purely hadronic process is illustrated by one of the decay modes of the D^+

$$D^+ \rightarrow \bar{K}^0 + \pi^+.$$

The forms of these decay modes hold a special significance at the LHC as they are the basic forms of often the more complex processes detailed in section 4.

At the LHC the direct production of W^+ will come predominantly from the interaction of $u\bar{d}$, with smaller contributions from $u\bar{s}$, $c\bar{d}$, and $c\bar{s}$. Conversely, the direct

production of W^- will come predominantly from the interaction of $d\bar{u}$, with smaller contributions from $d\bar{c}$, $s\bar{u}$, and $s\bar{c}$. The details of these interactions will be discussed in the following section.

2.2.2.1 The CKM Matrix

The CKM Matrix is a unitary 3x3 matrix which describes the so-called Cabibbo mixing angles between the quarks. The mixing angles essentially dictate the likelihood, or strength, of either a down-type quark decaying to an up-type quark or vice versa in flavor mixing weak interactions. The magnitudes of the CKM matrix elements to three significant digits are as follows, here neglecting the associated errors on the values.

$$\begin{bmatrix} |V_{ud}| & |V_{us}| & |V_{ub}| \\ |V_{cd}| & |V_{cs}| & |V_{cb}| \\ |V_{td}| & |V_{ts}| & |V_{tb}| \end{bmatrix} = \begin{bmatrix} 0.974 & 0.226 & 0.00359 \\ 0.226 & 0.973 & 0.0415 \\ 0.00874 & 0.0407 & 0.999 \end{bmatrix}$$

Fig 2. The CKM Matrix of Cabibbo mixing angles [1].

From this, for instance, we can see that the top quark decays to bottom approximately 99.8% of the time (the value of the matrix element squared). The notion of the particle generations is very striking when looking at the mixing angles and at the strong tendency of particles to convert within their generation as opposed to between the generations.

2.3 Strong Interactions and Hadronic Physics

The strong interaction is mediated by the massless spin-1 particles the gluons. A brief overview of the strong physics which will be important for our discussion is as follows.

2.3.1 Parton Model

Before the development of the quark model and the modern theory of quantum chromodynamics (QCD), protons (and neutrons) were modeled as being composed of point-like constituents called *partons*. In this model, instead of scattering off of the whole proton, an incoming particle would interact with, and scatter off of, a single parton within it. By this, each parton would carry only a fraction of the proton's total momentum given simply by the dimensionless variable

$$z = x \equiv p_1/P_1 \quad (2.3)$$

where p_1 is the parton momentum, and P_1 is the total proton momentum.

Another useful quantity is the squared energy-momentum transfer,

$$Q^2 \equiv (p - \mathbf{p}')^2 - (E - E')^2 \quad (2.4)$$

where the initial and final scattering particle has momenta and energies ($\mathbf{p}$, E) and ($\mathbf{p}'$, E') respectively [2, p.173].

2.3.2 Quark Model

The major problem which arises from the simplistic parton model is that it neglects the quark-gluon, and gluon-gluon, interactions. The fact that the quarks are not just isolated bodies adds additional energy and momentum exchanges to be taken into consideration in collisions, and can add entirely new particles to the system.

The likelihood of additional quark-gluon, and gluon-gluon, interactions scales as the strong coupling constant α_S per additional interaction vertex. As gluons possess color charge, their decay products can only be quarks. Strong interactions additionally conserve quark flavor and do not transmute quarks between generations. As gluons are neutral particles, their decay products must have a net neutral charge and so can only be a quark-antiquark pair.

2.3.2.1 Valence and Sea Quarks

With the introduction of the quark model of the proton, and of QCD, in addition to the so-called *valence* quarks of which the original partons accounted for, there are also the so-called *sea* quarks. Gluons are unique among the force carriers in that they are also capable of coupling to other gluons in addition to quarks. This comes about as they couple to any particle with color charge, which includes other gluons. The sea quarks are quark-antiquark pairs $q\bar{q}$ which arise from the quark-gluon interactions within the proton. Despite the theory progressing, the old terminology of partons remains.

2.3.2.2 Parton Distribution Functions

From deep inelastic scattering (DIS) experiments there have been developed so-called parton distribution functions for the various strongly interacting particles present in baryons. These include the valence quarks, gluons, and sea quarks. Parton distribution functions are weakly dependent on Q^2, and vary primarily with x. The functions are typically given in a form $xf(x)$, where $f(x)dx$ would be defined as the probability of finding the parton between x and x + dx. This can be seen pictorially for the valence

quarks, $\bar{u}$, and $\bar{d}$, in Fig. 2.1. In Fig. 2.2 we show the parton distributions for c, s, $\bar{u}$, and $\bar{d}$. As this also applies for $\bar{c}$, and $\bar{s}$, this latter comparison shows the weaker contributions that these heavier sea quarks have in the proton-proton interactions. This was one of the reasons that we excluded the charm and strange quarks from our final analysis of W+4jets.

These parton distributions come from the PDF CTEQ-6L1 [4]. This PDF was generated from DIS experiments from H1 and ZEUS, with additional information produced at DØ, by The Coordinated Theoretical-Experimental Project on QCD (CTEQ) collaboration. We used CTEQ-6L1 with $Q^2 = (100\text{GeV})^2$, which is an energy-momentum transfer on the order of the W mass, to produce all of our data and it is characterized by the equation

$$x\,f(x, Q_0) = A_0 x^{A_1}(1-x)^{A_2} e^{A_3 x}(1+e^{A_4 x})^{A_5}\ [4], \quad (2.5)$$

where the coefficients are experimentally derived fit parameters. This function was fit using $\alpha_S(M_Z) = 0.118$, cited as the Particle Data Group's average.

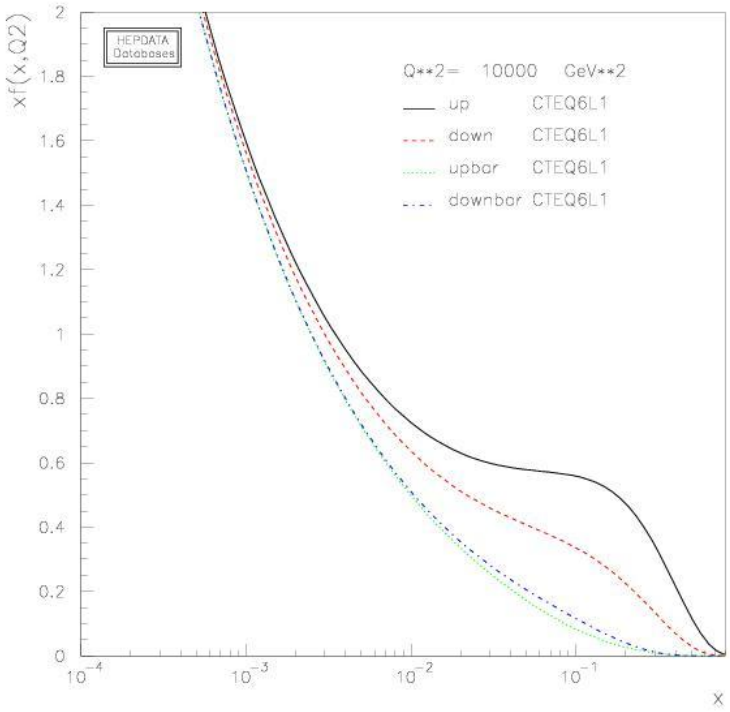

Figure 2.1 - CTEQ6L1 Parton Distribution for $ud\bar{u}\bar{d}$, created at $Q^2 = (100\text{GeV})^2$ [3].

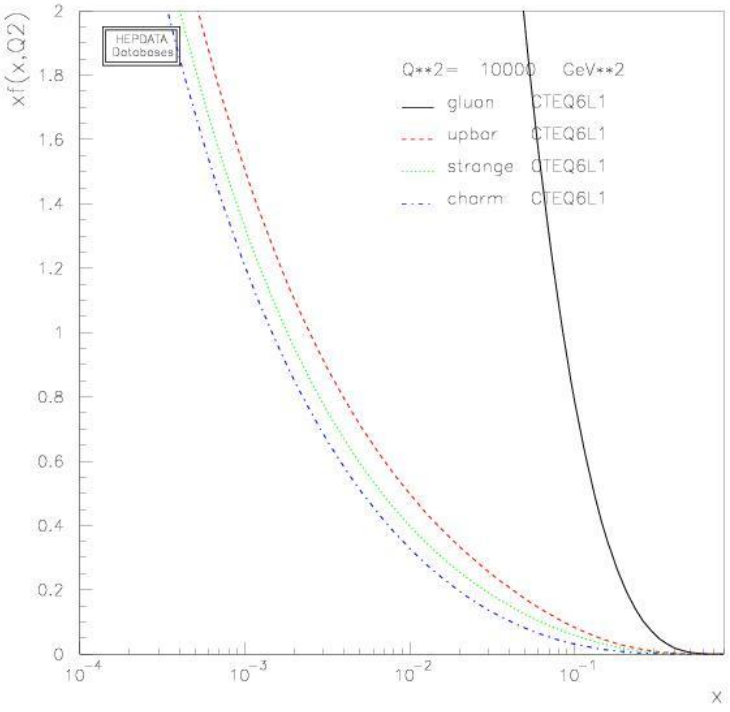

Figure 2.1 - CTEQ6L1 Parton Distribution for $g\bar{u}sc$, created at $Q^2 = (100\text{GeV})^2$ [3].

2.3.2.3 QCD Background

Another important strong phenomenon that we will not go into very deeply is the QCD background. Through quark-gluon and gluon-gluon interactions a multitude of hadronic particles are generated that are uninteresting to most physics studies but are important and significant background signals in collider physics. The QCD background is typified by a strong signal at lower energies which slowly dies down at higher energies. At the LHC the QCD background signal will most likely be highly troublesome due to large cross sections at high energies.

2.3.3 Hadronic Jets

An important phenomenon in hadronic physics are the jets. Due to the nature of the strong force, particles with color charge such as quarks and gluons are never found in isolation – there are no free quarks. As such, the quarks and gluons leaving an interaction go through a process called *fragmentation*, the constituents of which form the mesonic and baryonic "zoo" of particles observed in the detector. Fragmentation is a complex process that involves the formation of many hadronic daughter particles from the parent parton – a quark or gluon. These fragmentation constituents form a narrow "shower" of particles that follow nearly exactly the original trajectory of the initial quark or gluon. A jet is this shower of daughter particles originating from a parent parton. In this paper we will often denote "jets" as merely "j" especially in outlining specific processes.

3. Methods

Before going into the methods used there are a few key concepts that much be addressed. The first is a useful physical property used throughout collider physics are the notions of the rapidity, denoted y, and pseudorapidity, denoted η. These correlate to the polar angle θ of the particle's momentum vector off of the beam axis +z. However, where θ goes from 0 to π, rapidity and pseudorapidity go from +∞ to -∞, where y = η = 0 corresponds to θ = π/2, 90°.

Pseudorapidity, as defined in terms of the detector geometry is

$$\eta = -\ln[\tan(\theta/2)], \quad (3.1)$$

where θ is the traditional polar angle. Pseudorapidity, however, when put in terms of the particle's momentum takes on the form

$$\eta = \frac{1}{2}\ln\left(\frac{|p|+p_z}{|p|-p_z}\right) \quad (3.2)$$

which is a less relevant relationship in high energy collider physics, and will only act as an approximation to the true relativistic rapidity for light particles.

The rapidity, as defined in special relativity, is given as

$$y = \frac{1}{2}\ln\left(\frac{E+p_z}{E-p_z}\right) \quad (3.3)$$

which is the more useful quantity in that $\eta \approx y$ only when $m \ll p$ (here setting c = 1 for convenience). This can be seen through the relativistic mass energy relationship $E^2 = m^2c^4 + p^2c^2$. In high energy experiments the approximation can be used for particles of $\mathcal{O}(m_\mu)$ and less, but it breaks down for the measurement of massive particles such as $W^{\pm}$, Z^0, and top. This is especially noteworthy in that particles have a flat production distribution in y, but not in η.

Another important, but simple, concept is that of the transverse momentum. All this is are the components of the particle's momentum transverse, or perpendicular, to the beam – i.e. p_x, and p_y.

3.1 The ATLAS Detector

ATLAS, standing for A Toroidal LHC ApparatuS, is one of the two general purpose detectors at the LHC, the other being the Compact Muon Solenoid (CMS). Full details on the detector specifications can be found in The ATLAS Collaboration, G. Aad et al 2008. For this discussion we're mainly going to focus only on the specifications that directly affected our work. However, we will briefly describe the overall layout of the detector system for some point of reference as found in The ATLAS Collaboration, G. Aad et al 2008.

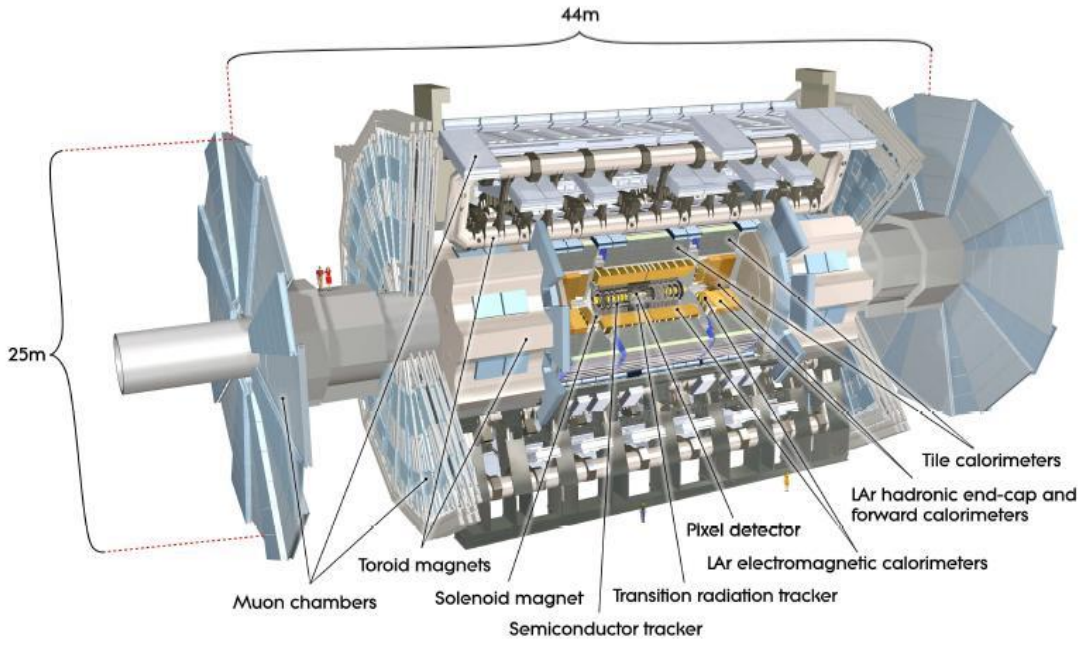

Fig 3.1 - The ATLAS Detector highlighting the key aspects of the detector system (The ATLAS Collaboration, G. Aad et al 2008).

ATLAS consists of three major subsystems - the inner detector, the calorimetry (CAL), and the muon spectrometer. The inner detector is a combination of pixel and strip detectors and has coverage out to $|\eta| < 2.5$, with electron recognition out to $|\eta| < 2.0$. The electromagnetic calorimetry system is a liquid Argon (LAr) based system primarily responsible for detecting photons and electrons (charged particles in general). The EM CAL has an eta range $|\eta| < 1.475$ for the "barrel" calorimeter, and $1.375 < |\eta| < 3.2$ for the end caps. The hadronic CAL has a tile calorimeter portion with main and extended barrels possessing $|\eta| < 1.0$ and $0.8 < |\eta| < 1.7$ coverage respectively. The tile CAL is cited as a sampling calorimeter using steel as the absorber with scintillating tiles as the active detector. The presence of high atomic number elements, such as iron, aids in the hadronic shower development. In addition are LAr based end cap and forward CALs with eta coverage $1.5 < |\eta| < 3.2$ and $3.1 < |\eta| < 4.9$ respectively. The muon spectrometer consists of four subsystems with eta coverage going out to $|\eta| < 2.7$ overall. The muon spectrometer consists of the resistive plate chambers $|\eta| < 1.05$, thing gap chambers between $1.05 < |\eta| < 2.7$, cathode strip chambers $2.0 < |\eta| < 2.7$, and monitored drift tubes $|\eta| < 2.7$.

3.1.1 Triggering

Although these systems have coverage out to these quoted values of the rapidity, they have a set value up to which they'll trigger on an event. The electron/photon trigger is set to $|\eta| < 3.0$, while the muon trigger is $|\eta| < 2.4$. The muon trigger will be important for our analysis as it defines up to what value of eta the asymmetry has

relevance in the detector. For instance, if the asymmetry peaks fall outside of $|\eta| = 2.4$ then they will be effectively undetectable, and therefore useless as an analysis tool.

3.1.2 Event reconstruction

Once an event has been detected, it must be reconstructed. This is a complicated process that we will summarize briefly. The CALs are one of the more straight forward detectors in that they are just designed to measure, or sample, the energy of the particles entering the CAL. They do this through various means as the particles dump their energy into the material of the CAL. This is why, for instance, the hadronic CAL uses high Z material in order to get the hadronic particles to interact and dump energy via nuclear interactions.

In addition to the energy, the particle's momentum must be measured. For charged particles, this is done by measuring their curvature in the toroidal and solenoidal magnetic fields with the pixel and strip detectors, and muon detector systems (additionally, from the curvature the charge of the particle is also measured). Muons are minimum ionizing particles and interact only through ionization trails, unlike photons and electrons which initiate electromagnetic cascades and strong particles which create hadronic cascades. The muon detection system was constructed as large as it was in order to gain a large enough lever arm to be able to measure the sagitta of the potentially TeV muons that will be produced.

Once the event has been triggered, and the particles have been detected and measured, the process of reconstructing the event which produced them begins. The computer hardware and software which do all the preprocessing is beyond the scope of

this paper, so we will just go over a number of the key features in the reconstruction process once an event has already been outlined.

Jet identification is one of the biggest parts of the reconstruction – identifying and associating the various hadronic particles with the same individual sources. This is usually accomplished based on the spread of the particles, and track analysis to try and converge particles to a similar origin. In addition to jet identification is the process of b-tagging in which one determines whether or not a jet originated from a b-quark. Although this is a standard tool in various event reconstruction channels, in our analysis we're trying to analyze the events based solely on their rapidity and are ignoring b-tagging.

Another very important part of the detection process is in determining the missing transverse energy (MET). Sometimes MET will be present just from either an incorrect measurement, or a missed particle(s), but it can also be due to energy and momentum being carried away from the system by an undetectable particle (in the Standard Model neutrinos). MET is triggered on directly by using the calorimetry. As the MET can only be reliably measured in the transverse plane it is thus not just regarded solely as "missing energy." MET channels will be very important in new physics searches in which we're looking for otherwise undetectable particles. If undetectable particles are created they will appear as MET in the system and can therefore be detected indirectly by their lack of detection. This includes many dark matter candidates and Super Symmetric (SUSY) Particles.

Once the leptons, jets, b-jets, and MET have been identified you are then able to go through a combinatoric recombination process to recover whether or not the constituents originated from a parent particle, such as a top quark, W, Z, Higgs, etc. This

is done by adding the 4-momenta of all the possibly associated daughter particles together and computing invariant masses etc. For instance, in reconstructing a purely hadronic top, you would add every jet in the event together in 3's, since in this case $t \to bjj$. You can easily make a routine that will loop through the particles in the events in this manner to search for invariant masses of the parents.

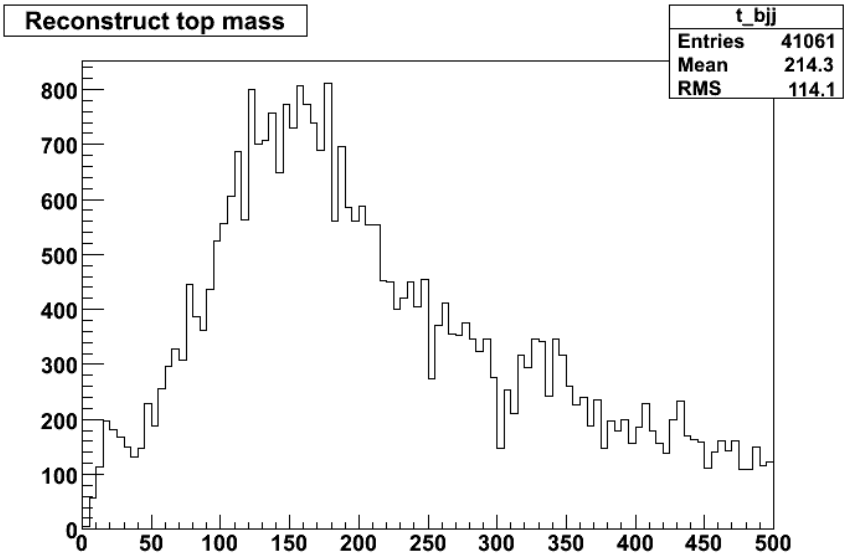

Fig 3.2 - Reconstruction of invariant top mass using ROOT, measured in events vs. GeV/c^2. Notice that the peak corresponds to the top mass $M_t = 171.2$ GeV/c^2 [1].

3.2 Simulation Methods

In lieu of actual data, you can also test ideas using simulated events, which is what we have done in our research (This is especially useful when no actual data exists yet!). Event generation is all done using Monte Carlo routines to attach the greatest level of realism onto what are essentially probabilistic physical processes.

The first stage of the simulation is integrating the matrix elements squared for the sub processes in the selected event at the parton level. This generates all of the outgoing

particle states – quarks, gluons, leptons, etc. but as such is in an unphysical condition due to the necessary hadronization of the strongly interacting particles.

The next level of the simulation is the parton shower in which the quarks and gluons are allowed to hadronize. This will often add additional jets onto the event as additional gluons, etc. are flung off of the event.

Finally, the last stage is in running the hadronized event through a detector simulation. This can be anything from a "pretty good simulation," which just imitates the detector specs, through to the fast simulation, all the way to the full simulation.

The fast simulation possesses a full model of the inner detector, but only simulates processes beyond that using "frozen showers" from a library table. These processes are just copied and pasted onto the simulation to emulate the interaction with the whole detector.

The full simulation is the next best thing to the detector itself. The full simulation models the complete detector, including its structure and composition down to the approximately the sub-mm level and models the particles traveling through the structure on that same scale. Needless to say, the full simulation takes about a great amount of computing power and time in order to run.

3.2.1 MadGraph, MadEvent

The matrix element calculator that we used was MadGraph [6]. The first step that MadGraph does is to generate all of the process diagrams – all variations, and sub processes of the process given – and produce the MadEvent code. MadGraph takes the incoming particles and runs them through the various PDF's and then determines all of

the possible reaction products. MadGraph has an easy to use web interface at the University of Illinois Urbana-Champaign High Energy website which is how I primarily prepared my process packages. However, by editing the proc_card.dat file you can specify what initial and final state partons you want. For instance, mandating that the process can only decay to $u\bar{u}, d\bar{d}$, and not to any strange or charm particles, the processes can be restricted in scope (arguably at a loss of some cross section, and perhaps a change in the observed physics). If these parameters are changed the Feynman diagrams will need to be regenerated using "new_process". After you've generated the diagrams that you require, you then are able to generate the events.

The event generation is handled by the program MadEvent. MadEvent simulates the outgoing particles from the process based on parameters set in the run_card.dat file. Here you are able to specify the number of events you want, the beam energy, minimum energies for various particles and jets, particle eta ranges etc. Events are then generated using "generate_events" and the selected number of unweighted events are produced in a Les Houches Events (LHE) format. These unweighted events files are what we used as our "theory" results. MadGraph/MadEvent is configured to be able to run on its own or in conjunction with PYTHIA and PGS and will automatically proceed with the PYTHIA and PGS simulation process if the pythia-pgs package is installed in addition to MadGraph 4.

3.2.2 PYTHIA

PYTHIA is the parton shower code which we used for our event generation. It was created by Torbjörn Sjöstrand, Stephen Mrenna, and Peter Skands [7]. We used the

PYTHIA-PGS package version 2.0.27 specifically designed to be loaded and run with MadGraph/MadEvent. PYTHIA takes the unweighted events LHE file from MadEvent and runs it through the parton showering procedure and then outputs the file again in an LHE format.

3.2.3 PGS

PGS, the Pretty Good Simulation [8] of high energy collisions, is the simulation software which we used for our analysis. The package was developed by John Conway of the University of California, Davis. Compared to the tremendous amount of time that the full simulator takes, pgs was able to simulate each 50,000 events sample in about an hour. We did these for each of the ten samples we're including in this report. The parameters which pgs used to emulate the detector are given in appendix A.1. Our PGS install came with our PYTHIA package and the two combined are designed to be run together with MadGraph. PGS takes in the hadronized events LHE file which PYTHIA output and goes through the simulation process outputting an LHCOlympics (LHCO) file. We then converted the LHCO files to ROOT ntuples using an LHCO to ROOT ntuple converter found in the MG/ME ExRootAnalysis package. These output files are what we used as our experimental simulation results.

4. Phenomenology

For each of the two processes which we studied, the events have a specific phenomenology which they follow. The following sections outline said phenomenology.

4.1 $W^{\pm}$ Production

The major focus of my project is on the asymmetry between the $W^{\pm}$ rapidity distributions which arise from the hadronic physics at the LHC being proton-proton (p-p). If the interactions were proton-antiproton (p-$\bar{p}$) as at the Tevatron this asymmetry would not exist as it does here. In p-$\bar{p}$ interactions, the direct W+ and W- will be produced predominately through interactions between the valence quarks and valence antiquarks. In these interactions the quark-antiquark pair will both have a similar x value and the W will be produced at rest.

The rapidity asymmetry at the LHC comes about due to W's being produced from valence quark – sea quark interactions, where the sea quarks constitute the antiquark required to produce the W as we saw in section 2.2.2. Specifically, the W^{+}'s exhibit a boost in their rapidity, y, arising due to the fact that the valence up quarks have, on average, a much higher x value than the sea down quark interacting with them. This difference in x is less pronounced for the valence down quarks, and as such the W^{-}'s exhibit a much weaker boost in eta. This difference can be seen in Fig. 2.1, the CTEQ-6L1 PDF.

The processes that we investigated were W+0jets, W+1jet, W+3jets, and W+4jets. For all of these we chose their leptonic decay mode with $W \rightarrow \mu + \nu_{\mu}$ being the specific leptonic decay mode chosen. We did this because we only wanted to focus on one type of lepton for simplicity. We chose the muon over the electron as they are simpler to register given that by the time they reach the outer muon detectors they will be the only charged particles to do so, in addition to not interacting through Bremsstrahlung or pair production which can complicate the reconstruction process. This is in addition to having

to identify the electrons from hadronic backgrounds which can sometimes mask any electrons which are present.

In our work, we made a prediction that after W+0jets the signal (asymmetry) would first get worse for W+1jet, and then get progressively better for each process thereafter. We made this prediction based on the notion that W+0jets would be the ideal case in which the W^+ would decay only with respect to the parton distributions of the initial state valence and sea quarks. W+1j would be the most unideal case in that the W would have the most momentum recoiling off of it in one direction. As this recoil in the lab frame would be isotropic in nature the W, and thus the lepton, would be randomly perturbed and the signal would disappear. As you progressively add additional jets, the added contributions would help balance the net momentum boost given to the W and the signal would begin to strengthen in turn. This is what we observe in the simulations.

The expected angular distribution of the lepton decay in the W's rest frame is quite complex and is more properly discussed in Acosta et al. 2004, and regardless is taken care of automatically by the generator. Due to this, even if the asymmetry persists for the W into W+4j, it may be blurred out due to the leptonic decay. For this reason, it was insufficient to merely look at the W at the "truth level" of the simulation and instead needed to follow the process through to the lepton decay and subsequent "smearing" in the detector simulation in order to have an accurate portrayal of the phenomena. As W+4j was our ultimate aim, the signal is characterized by $l + 4j + \mathrm{MET}$.

4.2 Top Production

The primary mechanism for top production is $gg \rightarrow t\bar{t} \rightarrow b\bar{b}W^+W^-$, in which the two colliding protons interact via gluons. From the CKM matrix element $|V_{tb}|$ we can see that top decays to bottom 99.8% of the time, and as such both tops will decay to bottoms in 99.6% of the reactions. As the primary top production comes from gluon-gluon, the top tends to be produced at rest as can be seen in the CTEQ-6L1 PDF, Fig. 2.2. From here, there are three decay modes possible, each depending on the W's decay mode.

In leptonic top, both W's decay to leptons, which is a very distinctive signal in a hadronic collider $l^+l^- + jj(b\bar{b}) + \text{MET}$. Although this decay signal is easy to trigger on, the usefulness of the event isn't as high as other decay modes. This comes about due to the presence of the two neutrinos generating a great deal of MET in the reconstruction of the event. The neutrinos prevent you from calculating the W's invariant mass, only allowing for the reconstruction of its so-called "transverse mass," M_{WT}. M_{WT} is calculated by the equation

$$M_{WT}^2 = 2\, pt_l\, pt_\nu\big(1 - \cos\big(\varphi_l - \varphi_\nu\big)\big), \quad (4.1)$$

where pt_l and pt_ν are the magntidues of the transverse 3-momenta of the lepton and neutrino, respectively, and the argument of the cosine is the angle between the lepton and neutrino. A plot of the W transverse mass can be seen in Fig. 4.1.

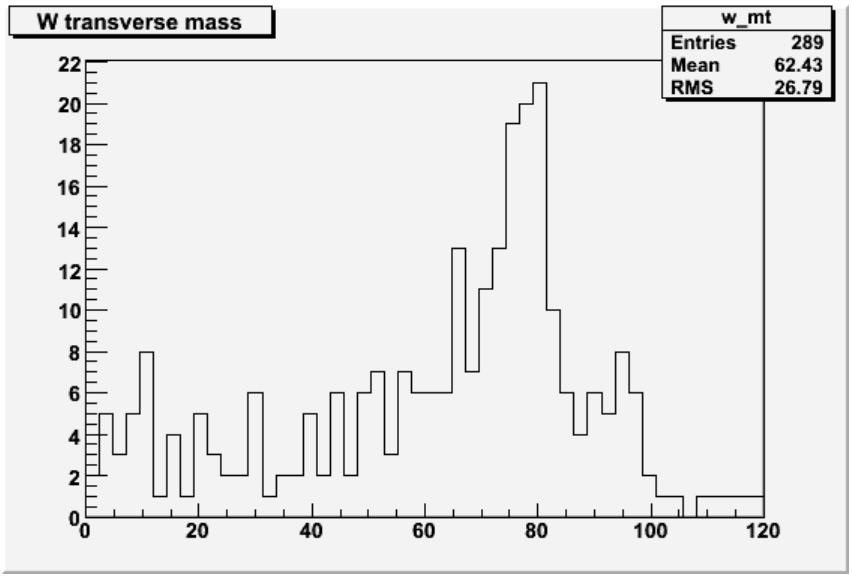

Fig. 4.1 - W transverse mass reconstructed using ROOT, measured in Number of Events vs. GeV/c^2.

It can be clearly seen how, after gradual increase, the transverse mass peaks at M_W, and then cuts off. This is unlike invariant mass reconstructions which follow a Gaussian distribution with a characteristic width Γ. The presence of the neutrino prevents the reconstruction of the W and in turn the parent top. Since in leptonic top this is the whole story, it becomes almost impossible to reconstruct the event. This is only made more difficult by the extra lepton-neutrino pair adding to the combinatorics. As can be seen, although leptonic top is easily triggered on, it is hard to reconstruct and therefore of limited value.

The most ideal decay mode on the reconstruction end is hadronic top, in which both W's decay hadronically. This decay chain is typified by 6 jets. In these events you have the greatest ability to reconstruct all constituent particles through combinatorics (ideally also combined with b-tagging), but run into other problems, the most major of which is triggering. In a hadron collider leptons are the odd balls being produced primarily through weak decays and therefore stand out quite strikingly from the jets. For

events in which all decay products are hadrons it is very difficult to pick out the signal events from the background. While this signal is useful in calibration of overall top quark production, it is less useful in calibrating noteworthy physics channels.

That leaves the most ideal mode for actual work – semi-leptonic top, in which one of the W's decays leptonically, and the other hadronically. This signal is thus seen as $l + 4j + \text{MET}$, the same as for W+4j. In this decay mode you get the best of both worlds – an ability to trigger on the event through the presence of the lepton, and the ability to reconstruct at least one of the tops from the hadronic decay. All that is involved is combinatorics in associating the correct b-quark with the right top and discounting any QCD background.

5. Results and Analysis

In generating our events were first found all of the processes and subprocesses with MadGraph, and then generated samples of 50,000 events with MadEvent. We used the default run_card.dat values for generating our processes with the exception of increasing the muon eta acceptance from 2.5 to 5.0. We did this in order to not cut out any of the events ultimately going into the PGS simulation, which would cut off any events undetectable in the actual detector anyways. Our simulation was at the full LHC beam strength of 7TeV apiece, 14TeV center of mass. For PGS we switched the default LHC pgs_card.dat to the ATLAS parameter card given in appendix A.1.

Initially in generating our processes with MadGraph we didn't restrict the incoming and outgoing partons (here the first two generations of quarks, and the gluon), though we did limit ourselves to muons and muon-neutrinos in the lepton channel. We

generated two samples for each process – W+njets, and $t\bar{t}$ – one for each W charge (dictating the outgoing muon charge). However, the full cross section of each W+4jets sample included 21,262 processes and sub processes (diagrams). This took approximately 36 hours to generate for each sample in MadGraph, and appeared as though over an additional week would be required in order to generate the desired number of events for each process in MadEvent. Due to various computing restraints, encountered problems and stability issues we were forced to truncate our incoming and outgoing partons to only include the first generation of quarks, and the gluon for W+4jets. This lowered the number of diagrams to 11756, which actually took only about 6 hours to generate in MadGraph and about 3 days to generate the 50,000 events in MadEvent.

We decided to cut out the charm, and strange quarks given that their PDFs exhibit a weaker cross section than $\bar{u}$ and $\bar{d}$, as can be seen in Fig. 2.2 However, as can also be seen is that in W^+ production by $c\bar{d}$ and $c\bar{s}$, and W^- production in $s\bar{u}$ and $s\bar{c}$, these reactions occur much more symmetrically with respect to x, and as such are produced mainly at rest. Regrettably, because of this our results as seen for W+4jets will be somewhat enhanced due to this truncated cross section. This shows up as a noticeable asymmetry for W^- production, and as a much sharper asymmetry for W^+ production.

5.1 Theory Results

Our theory results for W+0jets, W+1jet, W+3jets, W+4jets, and $t\bar{t}$ are as follows. In each of these plots, the cross section as measured in picobarns is plotted versus the eta of the particle.

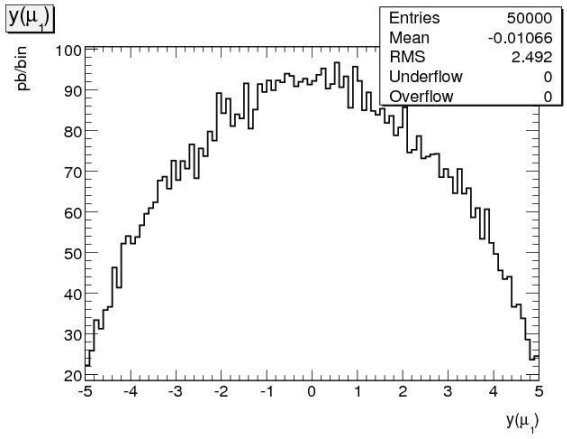

Figure 5.1.1 – μ^- production for W+0jets.

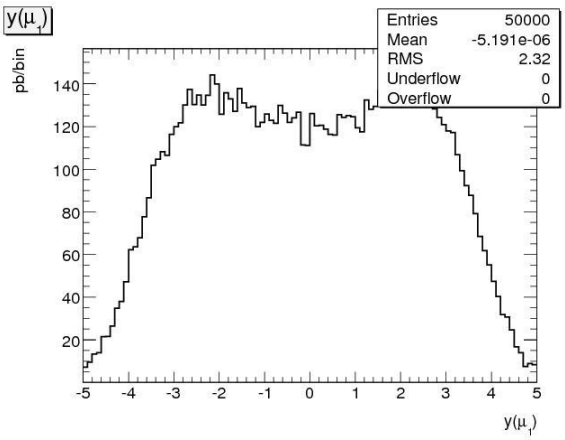

Figure 5.1.2 – μ^+ production for W+0jets.

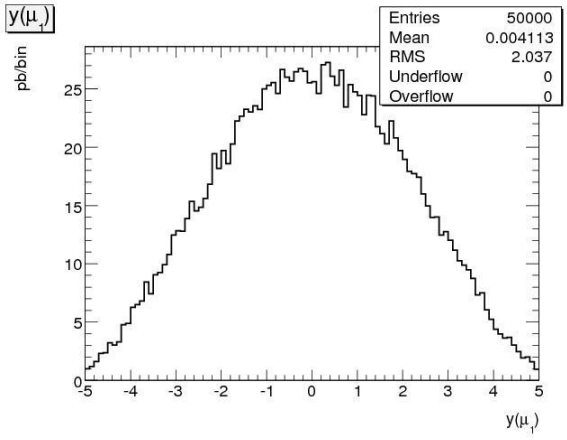

Figure 5.1.3 – μ^- production for W+1jets.

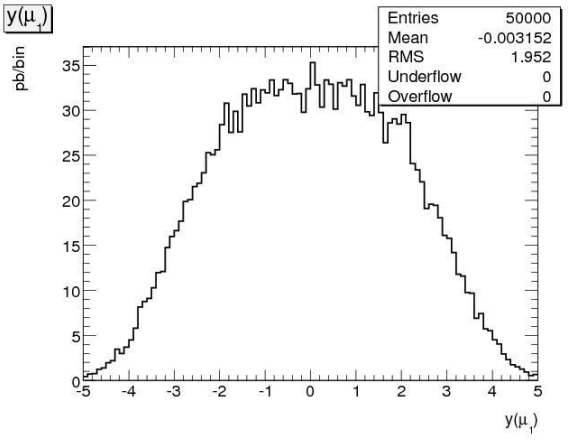

Figure 5.1.4 – μ^+ production for W+1jets.

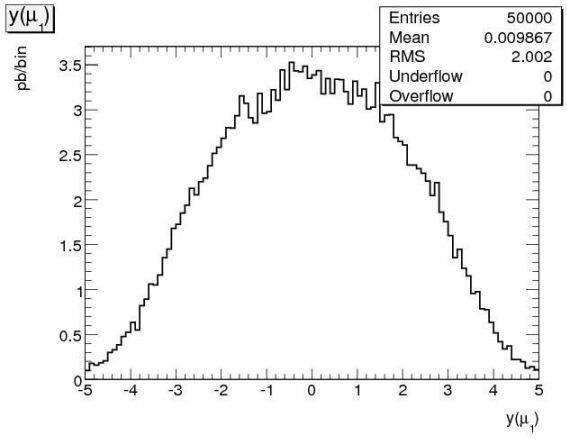

Figure 5.1.5 – μ^- production for W+3jets.

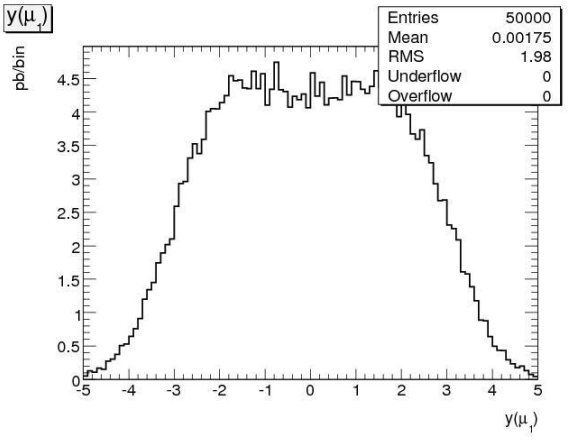

Figure 5.1.6 – μ^+ production for W+3jets.

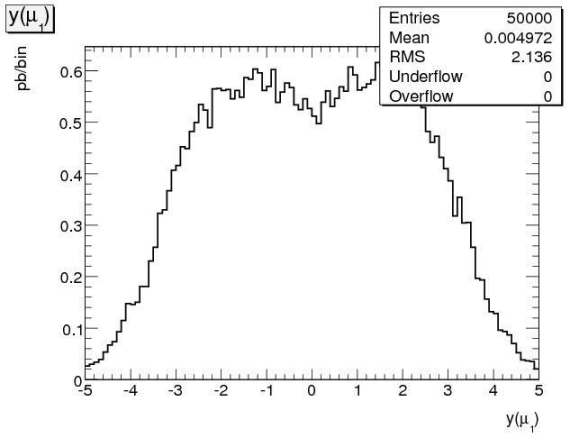

Figure 5.1.7 – μ^- production for W+4jets.

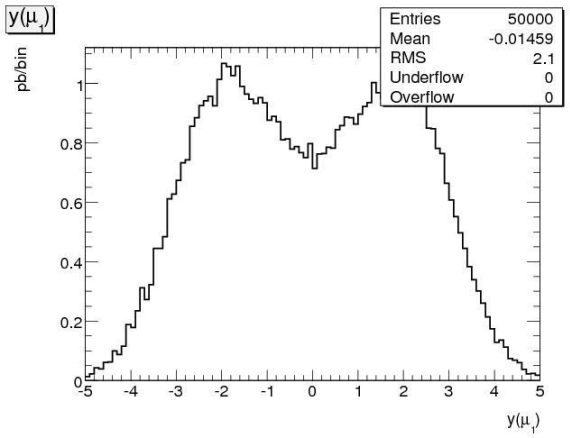

Figure 5.1.8 – μ^+ production for W+4jets.

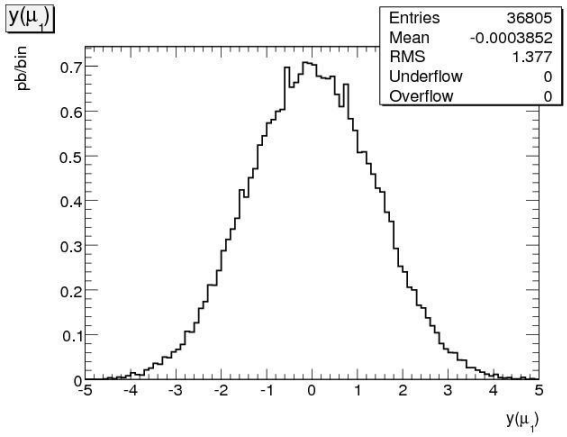

Figure 5.1.9 – μ^- production for $t\bar{t}$.

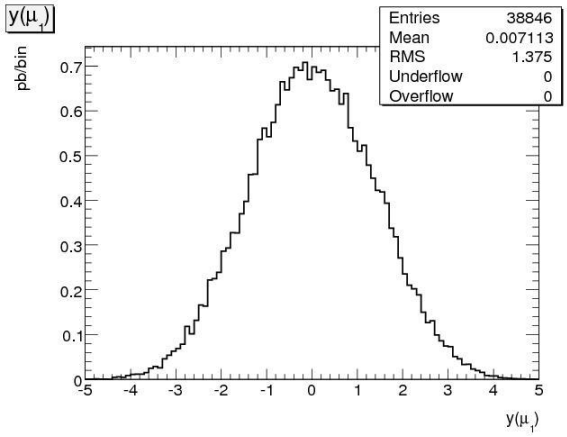

Figure 5.1.10 – μ^+ production for $t\bar{t}$.

Figs. 5.1.1-2 illustrate the assymetry of the W production as we see represented by the muon eta distributions. As stated as an assumption, the signal first weakens (homogenizes) for W+1jet and then gradually returns for subsequent numbers of jets. However, keep in mind once more that our W+4jets signals are both somewhat sharper than they should be due to the restriction mentioned above. A very important point to note is how the W^+ peaks peak before the muon eta cutoff of 2.4.

As can be seen in Figs. 5.1.1-2, the distributions of W+0jets are quite distinct compared to those seen in Figs. 5.1.9-10 for $t\bar{t}$. Notice also at how the $t\bar{t}$ distributions are virtually the same for either muon charge – they are symmetric.

Another trend to notice is the change in the cross sections involved in subsequent processes. For the W+njets, the cross sections begin very high and then drop by about a fourth for each additional jet until you arrive at W+4jets which has a similar cross section as $t\bar{t}$.

5.2 Experimental Results

Our experimental results for W+0jets, W+1jet, W+3jets, W+4jets, and $t\bar{t}$ are as follows. In each of these plots, the number of counts is plotted versus the eta of the particle.

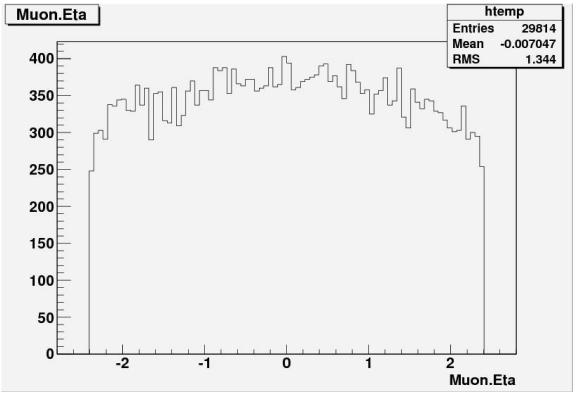

Figure 5.2.1 – μ^- production for W+0jets.

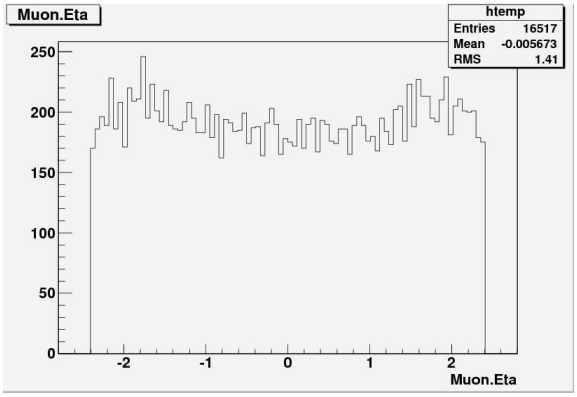

Figure 5.2.2 – μ^+ production for W+0jets.

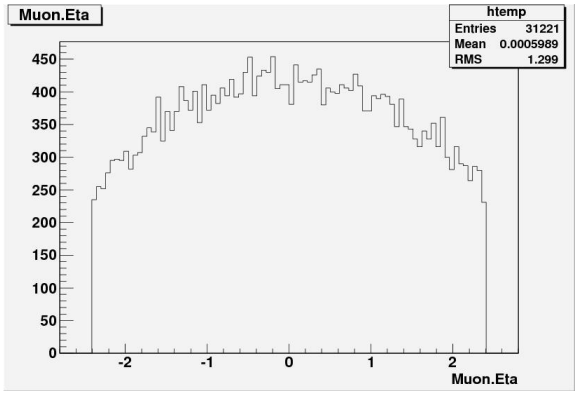

Figure 5.2.3 – μ^- production for W+1jets.

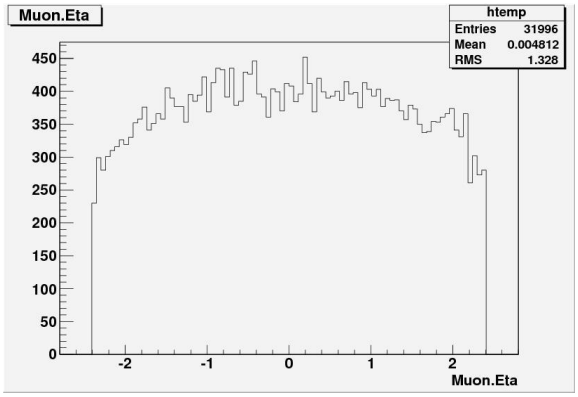

Figure 5.2.4 – μ^+ production for W+1jets.

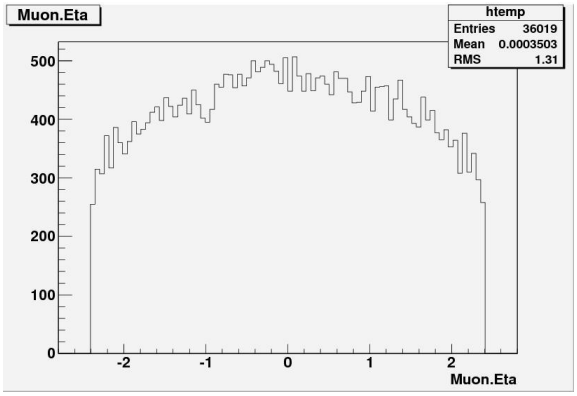

Figure 5.2.5 – μ^- production for W+3jets.

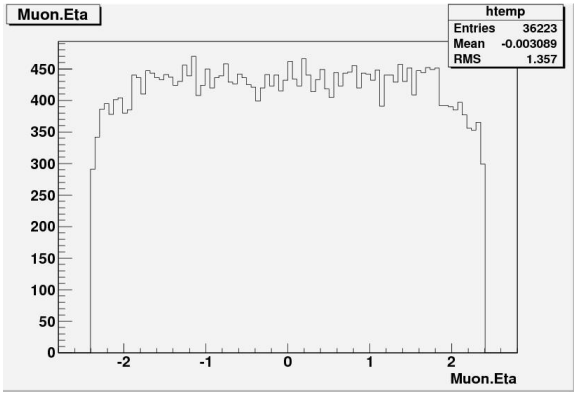

Figure 5.2.6 – μ^+ production for W+3jets.

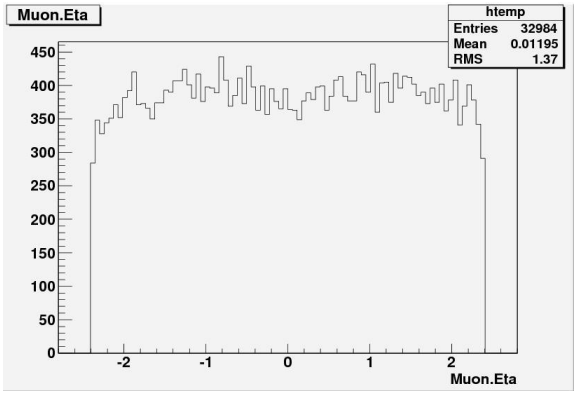

Figure 5.2.7 – μ^- production for W+4jets.

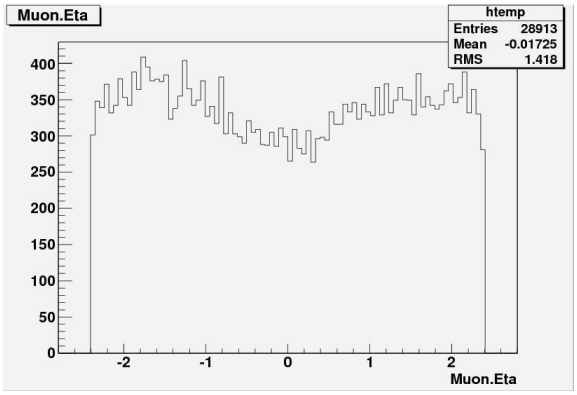

Figure 5.2.8 – μ^+ production for W+4jets.

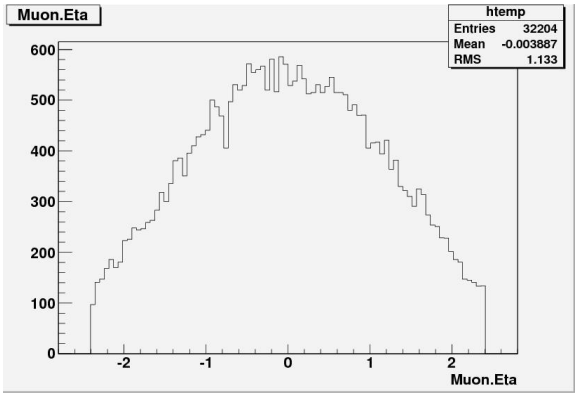

Figure 5.2.9 – μ^- production for $t\bar{t}$.

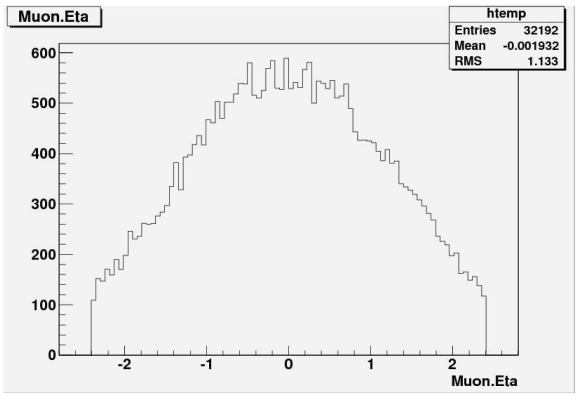

Figure 5.2.10 – μ^+ production for $t\bar{t}$.

As can be seen in Figs. 5.2.1-2, the assymetry is still somewhat present at the experimental level for W+0jets. Beyond which the assymmetry becomes generally unapparent until we again arrive at W+4jets. Although the signal at this level is no where as sharp as in the theory results, we can still see the assymmetry phenomena at the level of our analysis. Another very important distinction between W+4jets and $t\bar{t}$ is that still, even with a less apparent W assymetry, the distributions between the two events are quite distinct, with $t\bar{t}$ peaked, and W+4jets at worse flat, and at best with a local minimum at $\eta = 0$.

5.3 Fitting

The next step in our analysis would be to fit our signals. The fitting would be carried out in the ROOT environment, an object orientated data analysis framework developed by CERN [12]. Specifically, the RooFit package would be used to fit the individual signals. Once a fit is acquired, the W+4jets (±) and $t\bar{t}$ signals would be mixed together, based on the ratios of their respective cross sections, and we will attempt to

reextract each signal from the background. Additional considerations would also have to be put into the required cross section required before the signal could be fit.

6. Conclusion

As seen above, the W+4jets assymetry not only persists through to the theory level, but also extends into the experimental results for our chosen initial state partons. Despite our extended range of eta at the parton level, we see that the peaks of the W^+ distribution peak before the eta cutoff of the detector resolution. Once passed through the parton shower and the detector simulation, the distribution is still distinct from that of $t\bar{t}$. Due to the presence of this distinctive signature, given enough events it should be possible to fit our W+4jets, and $t\bar{t}$ signals from a combined signal.

Appendix

A.1 PGS pgs_card_ATLAS.dat

```
ATLAS           ! parameter set name
81              ! eta cells in calorimeter
63              ! phi cells in calorimeter
0.1             ! eta width of calorimeter cells  |eta| < 5
0.099733101     ! phi width of calorimeter cells
0.01            ! electromagnetic calorimeter resolution  const
0.1             ! electromagnetic calorimeter resolution * sqrt(E)
0.8             ! hadronic calolrimeter resolution * sqrt(E)
0.2             ! MET resolution
0.00            ! calorimeter cell edge crack fraction
cone            ! jet finding algorithm (cone or ktjet)
3.0             ! calorimeter trigger cluster finding seed threshold (GeV)
0.5             ! calorimeter trigger cluster finding shoulder threshold (GeV)
0.70            ! calorimeter kt cluster finder cone size (delta R)
1.0             ! outer radius of tracker (m)
2.0             ! magnetic field (T)
0.000005        ! sagitta resolution (m)
0.98            ! track finding efficiency
0.30            ! minimum track pt (GeV/c)
2.5             ! tracking eta coverage
3.0             ! e/gamma eta coverage
2.4             ! muon eta coverage
2.0             ! tau eta coverage
```

References

1. C. Amsler *et al.,* Physics Letters B667 (2008) 1
2. Martin, B.R., Shaw, G., Particle Physics. West Sussex, England: Wiley & Sons, 1992.
3. http://durpdg.dur.ac.uk/hepdata/pdf3.html
4. J. Pumplin, *et al.*, J. High Energy Phys. JHEP 07 (2002) 012
5. D. Acosta *et al.,* Physical Review D 70 (2004) 032004
6. J. Alwall, *et al.*, J. High Energy Phys. JHEP 09 (2007) 028
7. T. Sjöstrand, S. Mrenna, P. Skands, J. High Energy Phys. JHEP 05 (2006) 026
8. http://www.physics.ucdavis.edu/~conway/research/software/pgs/pgs4-general.htm
9. http://feyndiagram.com/
10. Williams, W.S.C., Nuclear and Particle Physics. New York, USA: Oxford University Press, 1990.
11. The ATLAS Collaboration, G Aad *et al.,* JINST 3 (2008) S08003
12. R. Brun, F. Rademakers, ROOT, Nucl. Inst. & Meth. in Phys. Res. A 389 (1997) 81-86.